Chemical Geology 635 (2023) 121622

Contents lists available at ScienceDirect

Chemical Geology

journal homepage: www.elsevier.com/locate/chemgeo

Mercury isotopes trace historical mercury pollution from Pb—Zn smelter in China

Kun Zhang [a,b], Liufeng Liao [c], Zhonggen Li [d], Yan Lin [e,*], Bo Meng [a,*], Xinbin Feng [a,b]

[a] State Key Laboratory of Environmental Geochemistry, Institute of Geochemistry, Chinese Academy of Sciences, Guiyang 550081, China
[b] University of Chinese Academy of Sciences, Beijing 100049, China
[c] Guizhou Ecometeorology and Satellite Remote Sensing Center, Guiyang 550002, China
[d] School of Resources and Environment, Zunyi Normal College, Zunyi 563006, China
[e] Tianjin Key Laboratory of Environmental Technology for Complex Trans-Media Pollution, College of Environmental Science and Engineering, Nankai University, Tianjin 300350, China

ARTICLE INFO

Editor: Hailiang Dong

Keywords:
Mercury pollution history
Mercury stable isotopes
Pb–Zn smelting

ABSTRACT

Lead–zinc (Pb—Zn) smelting is one of the largest anthropogenic emission sources of mercury (Hg) in China and the world. In the last few decades, Hg emission control devices have been employed in Pb—Zn smelters to reduce Hg emissions. To evaluate the effectiveness of Hg emission control, this study uses Hg isotopes to trace the sources of Hg in soils and reservoir sediments near the Zhuzhou smelter, the largest Zn production facility in China. The results showed that Hg concentrations in reservoir sediments were higher than those in soils at the three study sites, suggesting that reservoir sediments accumulate more Hg than soils do under the same conditions. Hg concentrations and deposition fluxes in reservoir sediments have dramatically decreased since the year 2000, suggesting the effectiveness of Hg emission control in the Zhuzhou smelter. Mercury isotope compositions in soil suggest binary mixing of Hg from the Zhuzhou smelter and the local background, and the contribution of Hg from the Zhuzhou smelter to soils and sediment is mainly a function of location and distance from the source. The model output suggested that approximately 61–75% of Hg in reservoir sediments was sourced from the Zhuzhou smelter. This study demonstrates that legacy Hg will continue to be a source to local ecosystems, even after Hg emission control has been implemented for decades.

1. Introduction

Mercury (Hg), a toxic heavy metal of adverse health risks to humans and ecosystems (Selin, 2009; Sonke et al., 2010; Yu et al., 2016; Zheng et al., 2018), has attracted global attention due to its long-range transport in the atmosphere, widespread deposition, and extensive bioaccumulation in ecosystems (Selin, 2009). Natural (e.g., volcano, wild fires) and anthropogenic (e.g., nonferrous metal smelting, coal combustion) activities both emit large amounts of Hg to the atmosphere in the form of gaseous oxidized Hg (GOM, Hg^{2+}), particulate bound Hg (PBM, Hg_P), and gaseous elemental Hg (GEM, Hg^0). GOM and PBM are readily deposited in the local environment via wet and dry deposition pathways, whereas Hg^0 has a long life of approximately 1 year in the atmosphere, allowing its transport globally (Driscoll et al., 2013). Lakes are an important sink for atmospheric Hg, and lake sediment cores are ideal natural archives for the reconstruction of atmospheric Hg deposition history (Kurz et al., 2019; Lepak et al., 2020).

Nonferrous metal (primary Al, Cu, Pb, and Zn) smelting is one of the largest anthropogenic Hg emission sources (Pirrone et al., 2010), accounting for 14.7% of global Hg emissions in 2018 (UNEP, 2019). Mercury pollution related to nonferrous metal smelting is a common environmental issue (Ma et al., 2013; Sonke et al., 2010), especially in China, the largest nonferrous metal producer and consumer in the world (Li et al., 2015; Zhang et al., 2011; Wu et al., 2016). A particular case can be found in the Zhuzhou smelter, the largest Pb—Zn smelter in China for decades (Li et al., 2011). Long-term Zn—Pb smelting of the Zhuzhou smelter has resulted in serious pollution of heavy metals (e.g., Hg, Pb, Zn and Cd) in the local environment (Li et al., 2018), with reported Hg concentrations of up to 2.27 ± 0.53 $mg \cdot kg^{-1}$ in surface soil (Li et al., 2011).

Since the early 2000s, China has commenced actions to decrease Hg emissions, including ceasing Hg mining activities and installing Hg

* Corresponding authors.
E-mail addresses: yan.lin@nankai.edu.cn (Y. Lin), mengbo@vip.skleg.cn (B. Meng).

https://doi.org/10.1016/j.chemgeo.2023.121622
Received 9 May 2023; Received in revised form 27 June 2023; Accepted 29 June 2023
Available online 3 July 2023

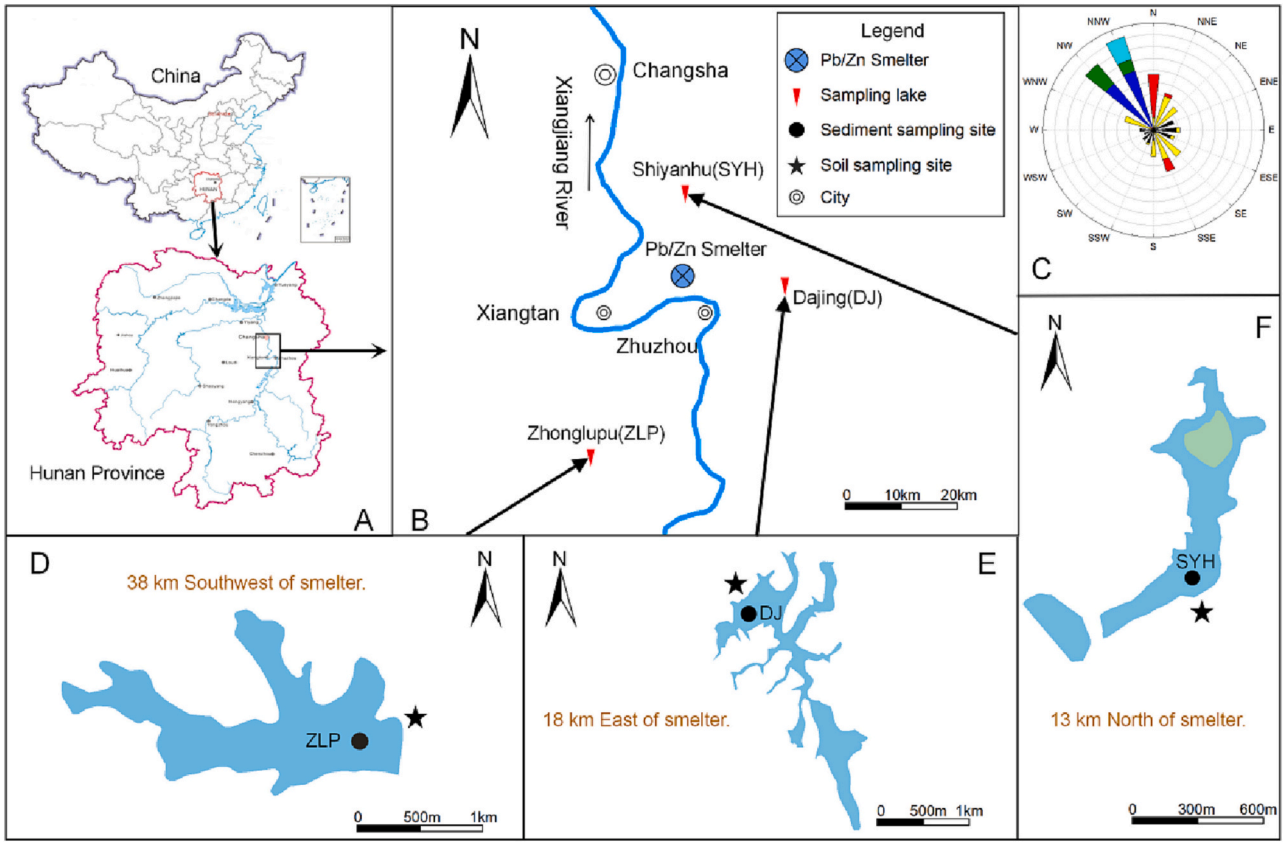

Fig. 1. Schematic map showing A) Location of the study area on the map. B) Location of the sampling point in the study area. C) Wind rose (wind direction frequency distribution of Zhuzhou in the last 20 years). D) ZLP reservoir. E) DJ reservoir. F) SYH Lake (the green area is an island in the lake). Brown words in D, E and F indicate the distance and location of the sampling lake to the Zhuzhou smelter. (For interpretation of the references to colour in this figure legend, the reader is referred to the web version of this article.)

reclamation towers in industrial sectors (Qin et al., 2020; Wang et al., 2010; Wu et al., 2014). Years of effort have resulted in a remarkable decrease in national-scale atmospheric Hg levels (Wang et al., 2010; Wu et al., 2014). The effects of Hg emission control on local ecosystems remain unclear, however. In Zhuzhou, although Hg emissions have remarkably decreased since the 2000s due to the installation of Hg reclamation towers (Wu et al., 2014), the large amounts of legacy Hg in the local environment may still be a threat to local ecosystems.

Mercury isotopes are useful tools for tracing the sources of Hg in the environment (Foucher et al., 2009; Feng et al., 2010; Yin et al., 2010a; Liu et al., 2011). The seven natural stable isotopes of Hg (^{196}Hg, ^{198}Hg, ^{199}Hg, ^{200}Hg, ^{201}Hg, ^{202}Hg, ^{204}Hg) can undergo unique mass-dependent fractionation (MDF, reported as δ^{202}Hg) and mass-independent fractionation (MIF, reported as Δ^{199}Hg and Δ^{200}Hg). (Bergquist and Blum, 2007, 2009). Various processes regarding Hg biogeochemical cycle (e.g., reduction, methylation, demethylation, volatilization, vaporization and adsorption) can trigger MDF (Bergquist and Blum, 2007; Zheng and Hintelmann, 2009; Estrade et al., 2009; Zheng and Hintelmann, 2010; Jiskra et al., 2012; Kritee et al., 2013; Perrot et al., 2013), while MIF mainly occurs during a few processes (e.g., aqueous Hg(II) photoreduction, methylmercury photodegradation, and Hg(0) volatilization) (Bergquist and Blum, 2007; Estrade et al., 2009; Sherman et al., 2010). However, Hg entering the environment through industrial activities probably has little to no MIF (Estrade et al., 2011). For example, Sun et al. (2013) reported that no MIF was observed during coal combustion. Another study by Yin et al. (2013a) indicated that no statistically significant MIF (Δ^{199}Hg ~ 0‰) was observed during the Hg ore roasting process. MDF and MIF processes result in distinguished Hg isotope signatures among geochemical Hg pools, which are of use in tracing the sources of Hg in the environment (Blum et al., 2014; Kwon et al., 2020).

Theoretically, long-term efforts of Hg emission control in the Zhuzhou area should have left changes in Hg isotopic composition in lake sediment cores. To examine the efficacy of control measures installed in the smelter during the period from 1991 to 2005, here we measured Hg isotopes in sediment cores collected from different localities around the Zhuzhou smelter and aimed to understand the historical variation in Hg sources.

2. Materials and methods

2.1. Study area and sampling sites

The Zhuzhou smelter (27°52′32.1594″N, 113°4′40.4394″E), located in northwestern Zhuzhou City, Hunan Province, South China (Fig. 1), was commissioned in 1956 and relocated to Hengyang City in 2018. It has been the largest Pb—Zn smelter in China for decades, and the ores consumed by this smelter are from Hunan Province and other parts of China (Li et al., 2011; Wu et al., 2014). From 1960 to 1968, 160 kt of Pb was produced, and approximately 2 t of Hg was released to the atmosphere from the Zhuzhou smelter without any control measures (Wu et al., 2014). Dust collectors and acid plants were installed in the Zhuzhou Smelter in 1969 and 1991, respectively. However, with the low efficiency of Hg removal and the growing production volume, approximately 95 t Hg was emitted from 1968 to 1990 (Wu et al., 2014). In 2003, approximately 34 t of heavy metals (e.g., Hg, As, Cd, Pb) was emitted into the local environment (Lei et al., 2008). The concentration of heavy metals in agricultural soil near the Zhuzhou smelter (e.g., Hg: 2.27 ± 0.53 mg·kg^{-1}. Pb: 723 ± 983 mg·kg^{-1}, Zn: 4731 ± 7352 mg·kg^{-1}, and Cd: 7.3 ± 7.6 mg·kg^{-1}) were found to be the highest in China (Li et al., 2011; Lei et al., 2008). Vegetables grown on nearby

farmland were also seriously contaminated by heavy metals (e.g., 2.4 ± 1.24 mg·kg^{-1} Hg in Chinese cabbage) (Liu et al., 2013).

Three reservoirs in Zhuzhou, including the Shiyanhu Reservoir (SYH), Zhonglupu Reservoir (ZLP) and Dajing Reservoir (DJ), were chosen for sampling in this study (Fig. 1). DJ and ZLP are located in water source protection areas, and SYH is located in a nature ecological reserve. In addition to the Zhuzhou smelter, no other Hg pollution source was found around SYH, DJ, and ZLP. Therefore, the Zhuzhou smelter is recognized as the predominant Hg source to the selected three reservoirs. Moreover, SYH, DJ, and ZLP are located in different directions of the smelter, and could suffer divergent Hg pollution status. SYH is located downwind of the second predominant wind, 13 km away from the smelter. ZLP and DJ are 38 km and 18 km away, respectively, from the Zhuzhou smelter, however they are not directly downwind of the smelter. The average water depths of DJ, ZLP, and SYH were 11 m, 8 m, and 15 m, respectively. As shown in Table S1 and Fig. S1, DJ, which was built in 1958, has a surface area of 2.64 km^2 and a watershed area of 52.00 km^2, and is surrounded by mountains and forests. ZLP, which was built in 1958, has a surface area of 0.68 km^2 and a watershed area of 31.61 km^2, and is surrounded by mountains and forests. SYH, which was constructed in 1957, has a surface area of 0.67 km^2 and a watershed area of 32.64 km^2 and is in the suburban area of Changsha City and predominantly surrounded by mountains and forests. As shown in Fig. S2, the forest coverage of the three watersheds was relatively stable from 1982 to 2018 (DJ: 66.2 ± 7.5%; ZLP: 66.4 ± 7.7%; SYH: 54.2 ± 8.5%, 2SD, $n = 37$).

2.2. Sample collection and preparation

In October 2021, three soil profiles (DJ: 60 cm; ZLP: 90 cm; SYH: 55 cm) were sampled near the three reservoirs (Fig. 1). The soil profiles were sliced into 5 to 10 cm intervals in the field using a precleaned ceramic cutter, preserved in plastic bags, and shipped to the laboratory. In October 2022, three sediment cores (DJ: 43 cm; ZLP: 45 cm; SYH: 39 cm) were collected from the three reservoirs using a custom-designed sampler (SWB-1, Wang et al., 1998). The sediment cores were sliced into 1 cm sections in the field using a precleaned ceramic cutter, preserved in plastic bags, and shipped to the laboratory. In the laboratory, the samples were freeze-dried (−40 °C), powdered and homogenized to a size of 200 mesh per inch using a mortar prior to chemical analysis.

2.3. Analytical methods

Radiometric dating of sediments using ^{210}Pb and ^{137}Cs methods was performed using a multi-channel spectrometer (GX6020, Canberra, USA) (Wu et al., 2022). Briefly, the ^{210}Pb, ^{226}Ra, and ^{137}Cs activities of sediment cores were measured via gamma spectrometry. The ages were calculated by the constant rate of supply (CRS) age model (Appleby and Oldfield, 1978; Sanchez-Cabeza and Ruiz-Fernández, 2012).

Total Hg (THg) concentrations of soil and sediment samples were measured by using a DMA-80 Mercury Analyzer (Milestone, Italy). Based on the THg concentration and age results, the Hg deposition flux (μg·m^{-2} yr^{-1}) was calculated based on Eq. (1):

$$Hg\ deposition\ flux = \left(C \times 10^{-3}\right) \times \left(GR \times 10^{2}\right) \times \left(BD \times 10^{-6}\right) \quad (1)$$

where GR is the growth rate (cm·yr^{-1}); BD is the dry bulk density (g·cm^{-3}); and C is the THg concentration (ng·g^{-1}). In this study, Hg deposition fluxes of the top and bottom samples of the sediment cores were not calculated due to the lack of deposition rates.

Thirty-six soil samples from three soil profiles ($n = 11$, 14, and 11 for DJ, ZLP, and SYH, respectively) and 127 sediment samples from three sediment cores ($n = 43$, 45, and 39 for DJ, ZLP, and SYH, respectively) were selected for Hg isotope analyses. Briefly, approximately 0.2 g of soil/sediment sample was digested with 5 mL of freshly prepared aqua regia (HNO_3/HCl = 1/3, v/v) in a water bath (95 °C, 3 h). The digestion solutions were diluted to 1 ng·mL^{-1} Hg before isotope analysis by Nu-Plasma II multi-collector inductively coupled plasma–mass spectrometer (Nu Instruments, Great Britain) (Yin et al., 2010b). NIST SRM 3133 was used as a working standard solution and measured in the same way as the samples. The MDF of the Hg isotope is expressed in $\delta^{XXX}Hg$ notation referenced to NIST-3133 (analyzed before and after each sample), in accordance with Eq. (2):

$$\delta^{XXX}Hg = \left[\frac{\left({}^{XXX}Hg/{}^{198}Hg\right)_{sample}}{\left({}^{XXX}Hg/{}^{198}Hg\right)_{NIST3133}} - 1\right] \times 1000 \quad (2)$$

where XXX is the mass number of each Hg isotope (199, 200, 201, and 202). The MIF is reported as Δ-values ($\Delta^{XXX}Hg$), which is the permitted deviation between the measured and theoretically predicted values of $\delta^{XXX}Hg$ (‰). Eqs. (3)–(5) give the relations used to calculate MIF as described by (Blum and Bergquist, 2007):

$$\Delta^{199}Hg\ (‰) = \delta^{199}Hg - \left(0.2520 \times \delta^{202}Hg\right) \quad (3)$$

$$\Delta^{200}Hg\ (‰) = \delta^{200}Hg - \left(0.5024 \times \delta^{202}Hg\right) \quad (4)$$

$$\Delta^{201}Hg\ (‰) = \delta^{201}Hg - \left(0.7520 \times \delta^{202}Hg\right) \quad (5)$$

Source apportionment analysis was performed by mixing models, which required accurate isotope values for each source and detailed information on the contaminated soil. In this study, a binary mixing model was established to evaluate the relative contribution of each source using Eqs. (6) and (7) (Yin et al., 2013b; Zhang et al., 2013):

$${}^{XXX}Hg_{sample} = {}^{XXX}Hg_{ant} \times X_{ant} + {}^{XXX}Hg_{nat} \times X_{nat} \quad (6)$$

$$X_{ant} + X_{nat} = 1 \quad (7)$$

Anthropogenic Hg originates primarily from industrial processes. Smelting Hg-bearing ores and burning fossil fuels probably produce a large range of MDF but little to no MIF (Estrade et al., 2011). Therefore, ${}^{XXX}Hg$ is Δ^{199}Hg in this study, and X_{ant} and X_{nat} are the contribution rates of Hg derived from anthropogenic and natural sources, respectively.

2.4. Quality control and statistical analysis

Quality assurance and quality control measurements consisted of method blanks, triplicates, and SRMs. Specifically, blanks and measurements of standard reference material (GSS-5: soil, Institute of Geophysical and Geochemical Exploration, certificated value: 290 ± 30 ng·g^{-1}; CC580: estuarine sediment, European Reference Materials, certificated value: 132 ± 3 mg·kg^{-1}) were analyzed after every ten samples. Regarding THg concentration analyses by the DMA-80 Hg analyzer, measurement of GSS-5 yielded THg recoveries of 101.8 ± 9.4% (2SD, $n = 13$). Analysis of CC580 yielded THg recoveries of 102.3 ± 8.2% (2SD, $n = 5$). All measurements of duplicate samples gave a relative standard deviation of <10%.

Regarding Hg isotope analysis, the uncertainties were determined by replicated analyses of samples and by repeated measurement of secondary standard solution (UM-Almadén) and digests of CC580. The overall average and uncertainty of UM-Almadén (δ^{202}Hg = −0.52 ± 0.07‰, Δ^{199}Hg = −0.02 ± 0.05‰, Δ^{200}Hg = 0.01 ± 0.05‰, Δ^{201}Hg = −0.02 ± 0.08‰, mean ± 2SD, $n = 16$) and CC580 (δ^{202}Hg = −0.53 ± 0.06‰, Δ^{199}Hg = 0.00 ± 0.04‰, Δ^{200}Hg = −0.01 ± 0.05‰, Δ^{201}Hg = −0.03 ± 0.08‰, mean ± 2SD, $n = 5$) are in agreement with those reported in previous studies (Janssen et al., 2015; Qin et al., 2020; Blum and Bergquist, 2007; Sun et al., 2016).

Statistical analysis was performed in Excel 2019 and SPSS Statistics 24 for Windows. One-way analysis of variance and an independent-samples t-test were performed to compare significant differences between two independent datasets, e.g., between different sampling sites (DJ, ZLP, and SYH) or different periods (before and after the

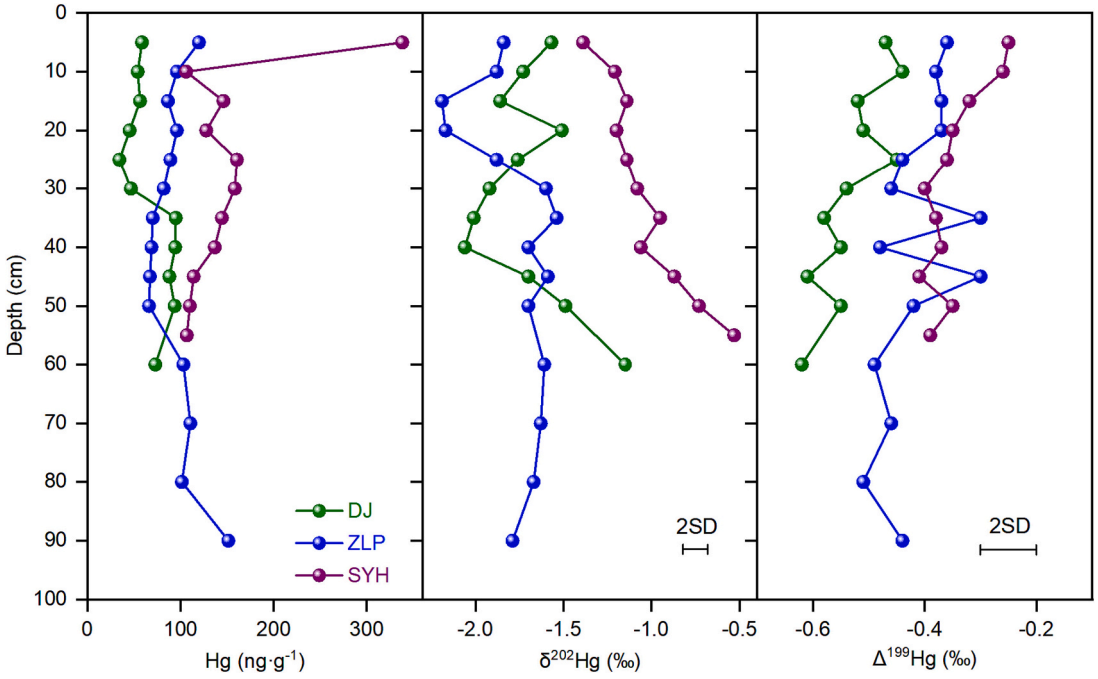

Fig. 2. THg concentration and isotopic composition in soil at three sites in Zhuzhou. 2SD represents two standard deviations of UM-Almadén, which are the same in the following figures.

commissioning of the Zhuzhou smelter). The determination coefficient (R^2) and significance differences (P) were computed for the linear regression fits. Significant differences were declared at a P value of <0.05. The data were plotted using Origin Pro 2018 and ArcGIS 10.3.

3. Results and discussion

3.1. Mercury concentration and Hg isotopic composition in soil profiles

The THg concentrations and isotopic compositions of the three soil profiles are shown in Table S2 and Fig. 2. Soil THg showed an increasing pattern: DJ (34.4–94.9 ng·g^{-1}; 67.3 ± 44.7 ng·g^{-1}, 2SD, $n = 11$) < ZLP (66.3–151 ng·g^{-1}; 93.5 ± 47.4 ng·g^{-1}, 2SD, $n = 14$) < SYH (106–338 ng·g^{-1}; 150 ± 131 ng·g^{-1}, 2SD, $n = 11$). The average THg concentration in soil profile of SYH was significantly higher than the geochemical background value of 68 ± 18 ng·g^{-1} in Changsha city, Hunan Province (Cheng et al., 2014), indicating the external Hg input. Moreover, the THg concentration in the topsoil (< 10 cm) of SYH was significantly higher than that of DJ and ZLP ($P < 0.01$), which can be explained by the distance (nearest) and location (downwind) of SYH to the Zhuzhou smelter. However, the average THg concentrations in soil profiles of DJ and ZLP were comparable with the geochemical background value (68 ± 18 ng·g^{-1}), suggesting that Hg input from the Zhuzhou smelter was less pronounced. DJ is surrounded by mountains, which limits the migration of Hg from the Zhuzhou smelter. ZLP is surrounded by a flat woodland. However, it is far from the smelter and not located in the main wind direction. These indicate that the migration and deposition of Hg emitted from the Zhuzhou smelter are mainly controlled by wind direction and distance. Additionally, topography can also affect the distribution of Hg in the study area.

The Hg isotopic composition of DJ and ZLP soil also shows a distinctive pattern from that of SYH soil (Fig. 2 and Table S2). Specifically, DJ soil shows δ^{202}Hg ranging from −2.06‰ to −1.15‰ (−1.71 ± 0.53‰, 2SD) and Δ^{199}Hg ranging from −0.62‰ to −0.44‰ (−0.53 ± 0.12‰, 2SD); ZLP shows δ^{202}Hg ranging from −2.19‰ to −1.54‰ (−1.77 ± 0.41‰, 2SD) and Δ^{199}Hg ranging from −0.51‰ to −0.30‰ (−0.41 ± 0.13‰, 2SD), and SYH shows δ^{202}Hg ranging from −1.39‰ to 0.53‰ (−1.03 ± 0.49‰, 2SD) and Δ^{199}Hg ranging from −0.41‰ to −0.25‰ (−0.35 ± 0.11‰, 2SD). Given the limited contamination by the Zhuzhou smelter, the Hg isotopic composition of DJ and ZLP soils were more negative. These data are comparable with previous studies on the isotopic composition of background soils (Feng et al., 2010; Liu et al., 2011). SYH soils are more contaminated with Hg from the Zhuzhou smelter. Consequently, the Hg isotopic composition of the SYH soils was more positive than that of the DJ and ZLP soils. The variations in δ^{202}Hg and Δ^{199}Hg in soil may reflect changes in Hg sources. However, Hg-MDF ubiquitously occurs during all biological, chemical, and physical processes, and it is difficult to directly use δ^{202}Hg for source tracing (Kwon et al., 2020). Instead, Δ^{199}Hg may be a useful Hg source tracer, given that Hg-MIF mainly occurs during photochemical processes with little

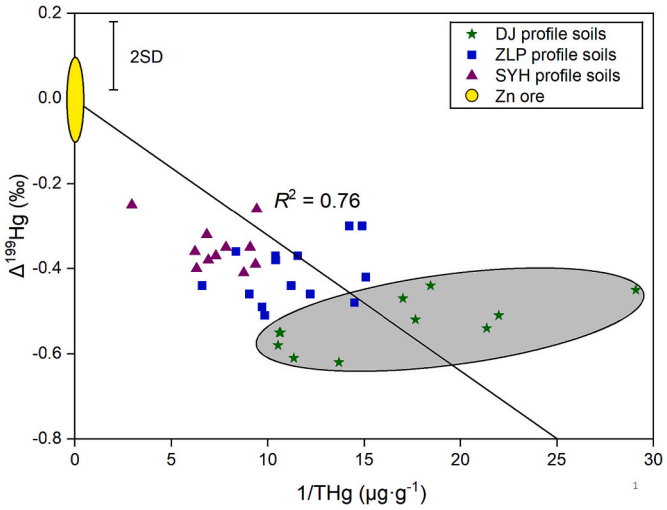

Fig. 3. Linear regression of Δ^{199}Hg (‰) vs 1/THg (μg·g^{-1}) between zinc ores and the three soil profiles near DJ, ZLP, and SYH, suggesting binary mixing of Hg from the Zhuzhou smelter (yellow area) and local background (gray area). (For interpretation of the references to colour in this figure legend, the reader is referred to the web version of this article.)

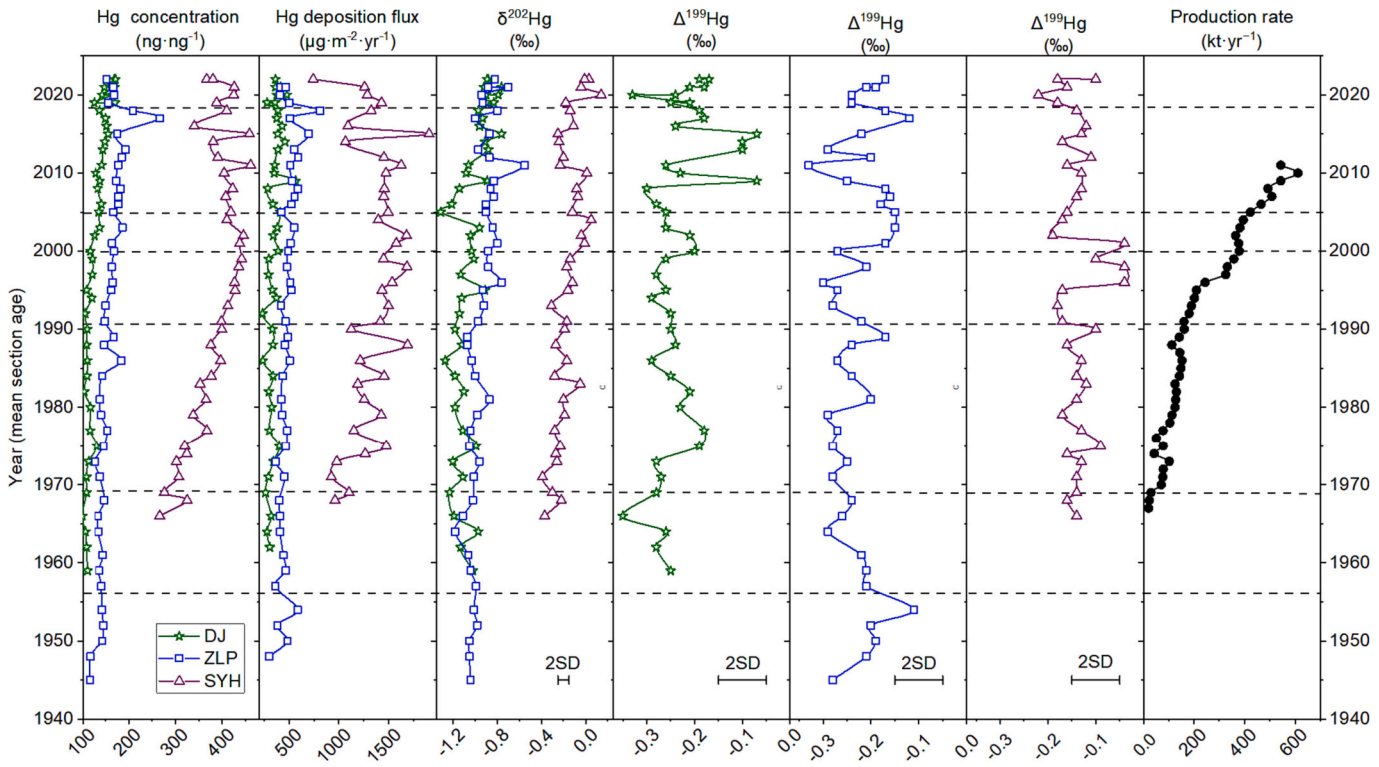

Fig. 4. Temporal variations in THg concentrations, Hg deposition fluxes, δ^{202}Hg, Δ^{199}Hg in DJ, ZLP, and SYH, and historical production rate values of the Zhuzhou smelter. The dates of important events for the Zhuzhou smelter are marked with horizontal dashed lines: (1) the Zhuzhou smelter first operated in 1956, (2) the dust collectors were installed in 1969, (3) the acid plants were installed in 1991, (4) two Hg reclaim towers were installed in 2000 and 2005, separately, and (5) the Zhuzhou smelter was relocated to another city in 2018. The horizontal dashed lines in the following figures represent the same events.

contribution from other reactions (Bergquist and Blum, 2007; Lepak et al., 2020). Here, the mean Δ^{199}Hg value (0.02 ± 0.06‰, 1SD, n = 102, Yin et al., 2016) of Zn ores from 102 Chinese zinc ore deposits was employed as the representative of the source signature of Hg emitted from the Zhuzhou smelter. Ore roasting processes do not trigger MIF (Yin et al., 2013a). The negative Δ^{199}Hg values of the Zhuzhou soil deviate from those reported for zinc ores, suggesting that the Zhuzhou smelter was not the sole source of Hg in the soil. Previous studies observed significantly negative Δ^{199}Hg values in background soils (Demers et al., 2013; Yin et al., 2016; Zheng et al., 2016). The bottom soil with the most negative Δ^{199}Hg (−0.62‰) in DJ soil profile may reflect the Hg isotopic signature of the background soil. The increase in soil Δ^{199}Hg from DJ and ZLP to SYH was likely due to an increase in Hg pollution from the Zhuzhou smelter. As shown in Fig. 3, a negative correlation between soil 1/THg and Δ^{199}Hg (R^2 = 0.76) suggests binary mixing of Hg from two major Hg sources: the Zhuzhou smelter and the local background soil. We used Δ^{199}Hg as a tracer to quantify Hg contributions from different sources (Sun et al., 2020). Based on Eqs. (6) and (7), the source signatures of the Zhuzhou smelter (Δ^{199}Hg = 0.02 ± 0.06‰) and the local background soil (Δ^{199}Hg = −0.62‰) and the mean Δ^{199}Hg values of DJ soil (−0.53 ± 0.13‰, 2SD, n = 11), ZLP soil (−0.41 ± 0.13‰, 2SD, n = 14), and SYH soil (−0.35 ± 0.11‰, 2SD, n = 11), we estimated that ~13 ± 9% (1SD, 0% to 28.1%), ~32 ± 11% (1SD, 17.2% to 40.6%) and ~ 42 ± 9% (1SD, 33.6% to 58.6%) of Hg in DJ, ZLP and SYH soils, respectively, was sourced from the Zhuzhou smelter.

3.2. Mercury pollution in reservoir sediments

The historical variations in THg concentration in sediment cores from DJ, ZLP, and SYH are shown in Table S3 and Fig. 4. The THg concentrations showed a similar increasing pattern with the soil: DJ (98.1–171 ng·g^{-1}; 129 ± 42.5 ng·g^{-1}, 2SD, n = 43) < ZLP (115–266 ng·g^{-1}; 159 ± 52.5 ng·g^{-1}, 2SD, n = 45) < SYH (266–461 ng·g^{-1}; 385 ± 99.2 ng·g^{-1}, 2SD, n = 39). THg concentrations in the cores show similar temporal trends. Here, it is worth noting that the THg concentrations of reservoir sediments are higher than those of soils at each site (P < 0.01, Fig. S3), implying that anthropogenic perturbations and runoff could release and transport Hg from soil to sediment. Therefore, lake sediment can be recognized as a better natural archive to record Hg pollution history than soil profiles.

Hg deposition flux shows similar patterns to THg concentration, which increased during the 1960s to 1990s and slowly decreased afterward (Fig. 4). Hg deposition fluxes of the three reservoirs were as follows: DJ, 231.0 to 565.7 μg·m^{-2}·yr^{-1} with a mean value of 349.7 ± 130 μg·m^{-2}·yr^{-1} (2SD, n = 41); ZLP, 297.6 to 809.8 μg·m^{-2}·yr^{-1} with a mean value of 482.2 ± 178 μg·m^{-2}·yr^{-1} (2SD, n = 43); and SYH, 741.9 to 1906.4 μg·m^{-2}·yr^{-1} with a mean value of 1349.7 ± 492 μg·m^{-2}·yr^{-1} (2SD, n = 37). An increase in the Hg deposition flux in SYH began in approximately 1970 when the Zhuzhou smelter was commissioned. Hg deposition flux at SYH was significantly higher than that at ZLP (P < 0.01) and DJ (P < 0.01), perhaps a result of the commission of the Zhuzhou Smelter increasing the Hg deposition flux in the environment. From 1969 to 1990, although dust collectors were installed in the smelter, 90% of the Hg (Hg^{2+}, Hg^0, and PBM) was emitted into the atmosphere due to the low efficiency of Hg removal and the growing production volume (Wang et al., 2010; Wu et al., 2014). During this period, THg concentrations and deposition flux showed an increasing trend, particularly in SYH, which is most sensitive to Hg emissions from the Zhuzhou smelter. From 1960 to 1990, THg concentrations in SYH showed a significant positive correlation with production (Wu et al., 2014) (R^2 = 0.67), indicating that Hg in sediments was mainly derived from the smelter during this stage (Fig. 4). With technological improvements, an acid plant was installed to recover SO_2 as H_2SO_4 in 1991, and two Hg reclamation towers (Boliden-Norzink) were installed to recycle Hg in two Zn smelting lines in 2000 and 2005. In the Hg reclamation tower, Hg vapor was oxidized to form mercurous chloride by

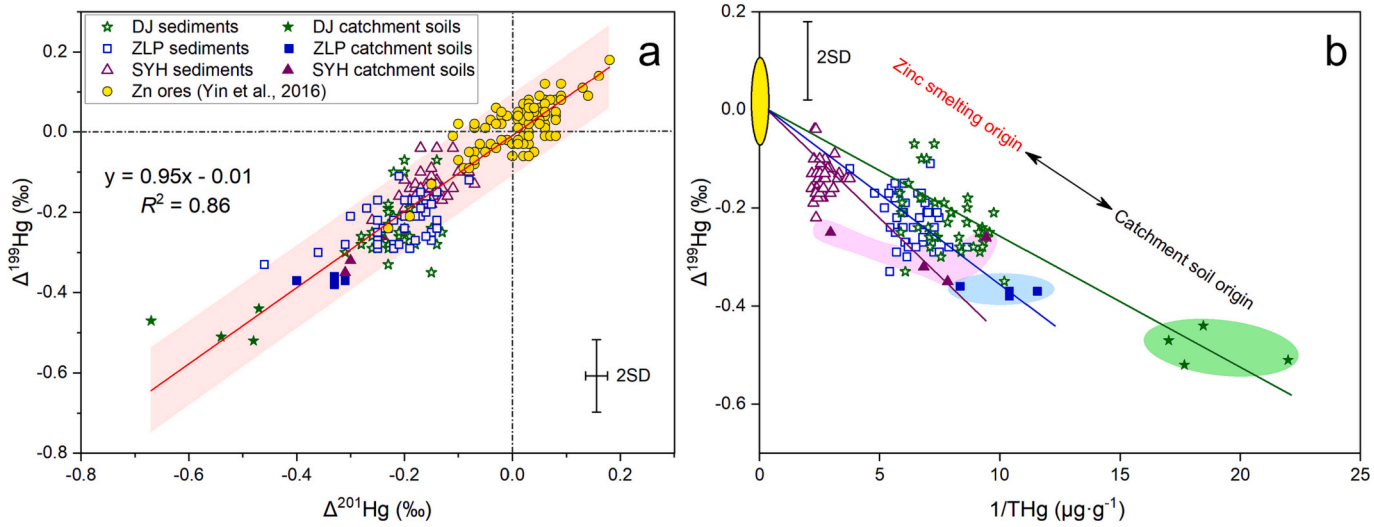

Fig. 5. Mercury isotope plots of samples: a) Linear regressions of Δ^{201}Hg vs Δ^{199}Hg in catchment soil, reservoir sediment and Zn ore samples. The fitted lines (red) are bound by 95% confidence bands; b) Δ^{199}Hg vs 1/THg in catchment soils, sediments and Zn ores. The yellow area represents the range of Zn ores (Yin et al., 2016). The three catchment soils are marked with different colour zones. (For interpretation of the references to colour in this figure legend, the reader is referred to the web version of this article.)

mercuric chloride (Wang et al., 2010). Mercurous chloride is insoluble and precipitates as calomel, which can be recycled efficiently. The average Hg removal efficiency of the Hg reclamation process was 88% in this process (Wang et al., 2010). Thus, although the annual production of Zn and Pb rapidly increased (3.6-fold) after the 1990s ($P < 0.01$), Hg emissions were <8% of the historical total emissions of the smelter due to these efficient Hg reclamation technologies (Wu et al., 2014). After the 1990s, THg concentration and Hg deposition flux in the three sediment cores did not increase significantly compared to the significant increase in Pb—Zn production in the Zhuzhou Smeter. Specifically, after 2000, THg concentrations and deposition fluxes in SYH showed a descending trend, indicating the effectiveness of the control measures in reducing Hg emissions.

Distance and wind direction are important factors in controlling the extent of atmospheric Hg deposition (Sakata and Marumoto, 2005). In the study area, the annual dominant wind direction was north–northwest (Fig. 1). For the three sampling sites, SYH is the only reservoir located downstream from the dominant wind direction of the Zhuzhou smelter, and represents the highest average THg concentration in the sediment. A previous study showed that THg concentration in surrounding soils of the dominant wind direction was higher than that of other directions, and gradually decreased with the increasing distance from the Zhuzhou smelter (Wu et al., 2014). Therefore, it is reasonable that the historical Hg deposition flux of the sediments in SYH is more responsive to Hg emission control measures of the smelter. The Hg deposition flux of SYH was significantly higher than that of ZLP ($P < 0.01$) and DJ ($P < 0.01$) due to its location downwind of the second predominant wind and the nearest distance to the Zhuzhou smelter. In the absence of control measures, the Hg deposition flux in SYH increased continuously as the smelter output increased (Fig. 4). In 1988, the Hg deposition flux in SYH reached 1690 $\mu g \cdot m^{-2} \cdot yr^{-1}$, which was 1.8 times the value in 1971. Subsequently, the Hg deposition flux in SYH did not increase or even decreased after the introduction of the acid plant and Hg reclamation towers after 1990 (Fig. 4). This highlights the role of control measures in reducing Hg contamination. Notably, after the relocation of the Zhuzhou smelter to another city in 2018, THg concentrations and deposition fluxes in the three sediment cores showed a declining trend (Fig. 4).

3.3. Sources of Hg in reservoir sediments

As shown in Fig. 4, Hg isotopic compositions are largely variable in sediment cores from DJ (δ^{202}Hg: −1.31‰ to −0.76‰, −1.03 ± 0.28‰; Δ^{199}Hg: −0.35‰ to −0.07‰, −0.23 ± 0.13‰; 2SD, n = 43), ZLP (δ^{202}Hg: −1.18‰ to −0.55‰, −0.94 ± 0.23‰; Δ^{199}Hg: −0.33‰ to −0.11‰, −0.22 ± 0.10‰; 2SD, n = 45), and SYH (δ^{202}Hg: −0.39‰ to 0.14‰, −0.16 ± 0.24‰; Δ^{199}Hg:–0.22‰ to −0.04‰, −0.14 ± 0.08‰; 2SD, n = 39). Compared to DJ and ZLP sediments, the δ^{202}Hg and Δ^{199}Hg values in SYH sediments are closer to those of Chinese Zn ores (Yin et al., 2016), suggesting a great influence by the Zhuzhou smelter at SYH. For more conservative Δ^{199}Hg, a slight negative Δ^{199}Hg shift in ZLP and SYH occurred in approximately 1990. This could be a result of the installation of acid plants in 1991. As the most polluted reservoir, the positive Δ^{199}Hg shift in approximately 1995 in SYH sediment core is likely a result of the sharp increase in production of the Zhuzhou smelter. However, the negative Δ^{199}Hg shift after 2000 indicates the effect of the Hg reclaim towers installed in 2000 and 2005 in reducing Hg emissions.

As shown in Fig. 5a, the slope of Δ^{199}Hg to Δ^{201}Hg was 0.95 in the soil, sediments studied. This suggests that Δ^{199}Hg is a robust indicator to discriminate Hg sources in the sediment of the three reservoirs (Schneider et al., 2021). The Δ^{199}Hg values in the soil and sediment both show the same pattern: DJ < ZLP < SYH < Zn ore. Here, we again used the linear relationship of Δ^{199}Hg and 1/THg to indicate the Hg contamination source of sediments (Fig. 5b). Topsoil can reflect short-term (decadal to centennial) variations (An et al., 2022). In the three soil profiles, the Δ^{199}Hg was relatively stable in the topsoil (0 and 20 cm, Fig. 3) and thus was selected to represent the isotopic composition of the catchment soil endmember. As shown in Fig. 5b, the sediment samples in DJ, ZLP and SYH were located between Zn ores and their catchment soils, indicating that Hg in the sediments was the mixing of zinc smelting and each catchment soil. In addition, the Δ^{199}Hg values in the catchment soil and the sediment both show the same pattern: DJ < ZLP < SYH < Zn ore, again indicating that SYH, the closest reservoir to the Zhuzhou smelter, is the most seriously polluted by Hg from the smelter. In the study area, Hg emitted from the smelter carried the same isotopic signal as Zn ore (Δ^{199}Hg = 0.02‰), while the Δ^{199}Hg value of background soil (Δ^{199}Hg = −0.62‰) was much less than that of Zn ore. Based on the source signature of Δ^{199}Hg for the Zhuzhou smelter and catchment soils from each site, we used Δ^{199}Hg as a conservative tracer

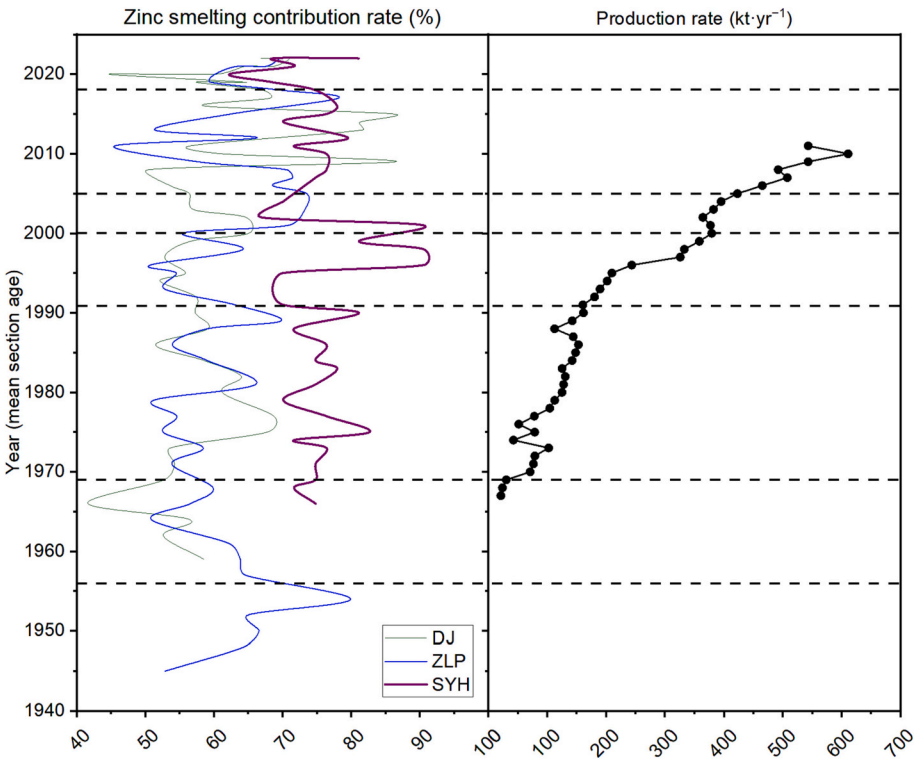

Fig. 6. Temporal variations in zinc smelting contribution in sediment cores of DJ, ZLP, and SYH and historical production rate values of the Zhuzhou smelter.

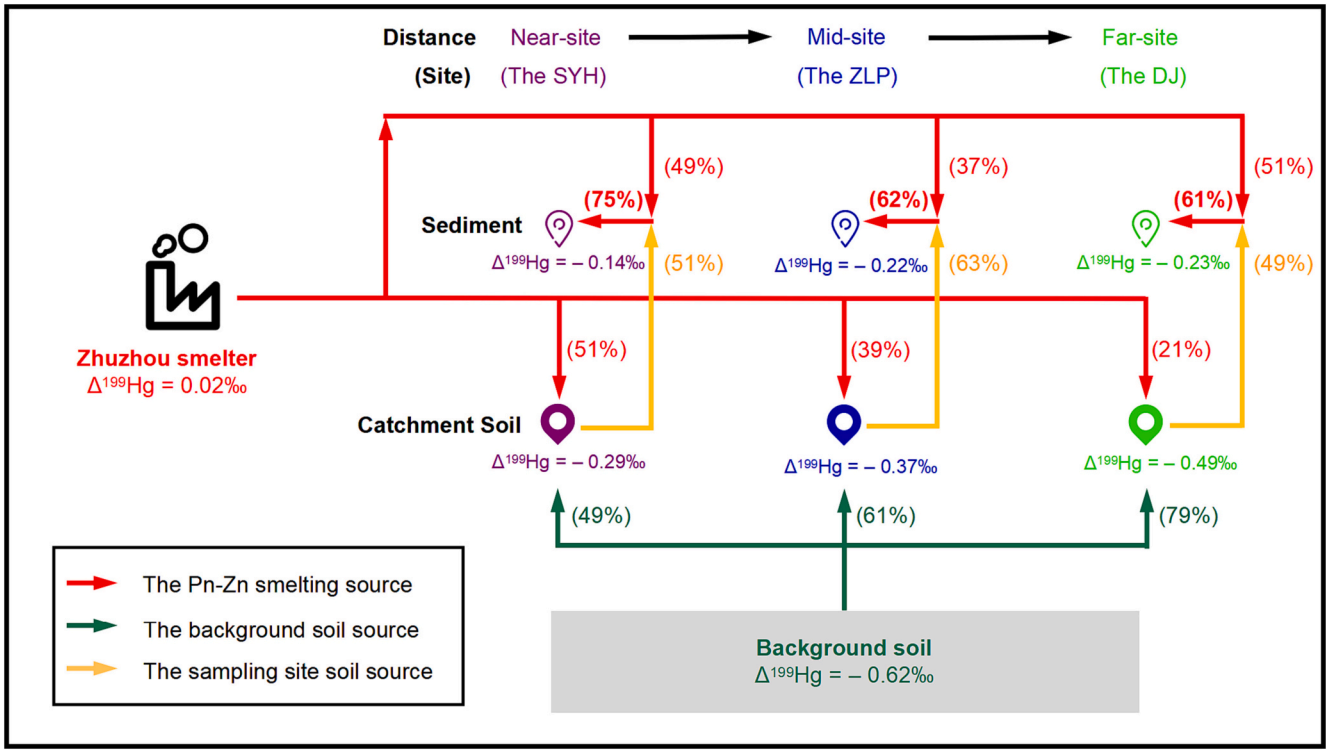

Fig. 7. Conceptual model showing the sources of Hg in soil and sediments at three study sites. The red, green, and yellow arrows indicate that Hg comes from the smelter, the background soil, and the soil runoff, respectively. (For interpretation of the references to colour in this figure legend, the reader is referred to the web version of this article.)

to build a binary mixing model to quantify Hg contributions from different sources, employing Eqs. (6) and (7). The model outputs indicate that the zinc smelting source from the Zhuzhou smelter was responsible for the different contribution rates of Hg in the SYH, ZLP and DJ sediments throughout history (Fig. 6). The most polluted reservoir, SYH, has historically been exposed to the most Hg from zinc smelting. In

the early smelting activities (~ 1969), the contribution rate of Hg from the Zhuzhou smelter to the SYH sediments was 74.8%, which was 1.41 times that of DJ and 1.24 times that of ZLP. In 1996, with increasing production of the Zhuzhou smelter and the lack of control measures, the contribution rate of Hg from the Zhuzhou smelter reached 91.3%, which was 1.72 times and 1.80 times higher than that of DJ and ZLP, respectively. However, with the improvement of Hg emission reduction technologies and measures, the contribution rate of Hg from the Zhuzhou smelter decreased to 71.1% in 2005, and there was no significant increase in the following years. Our data, overall, highlight the significant role of control measures in Hg emission reduction throughout history.

As the major source of Hg pollution, the Zhuzhou smelter contributed an average of ~75%, ~62% and ~ 61% of Hg in the SYH, ZLP and DJ sediments, respectively (Fig. 7), consistent with the decreased pattern of THg at the three sites.

4. Conclusions

This study reconstructed the pollution history of the largest Pb—Zn smelter in China in the surrounding environment. The results clearly illustrated the different pollution of the smelter on the surroundings: the highest THg concentrations and Hg deposition fluxes were found to begin increasing immediately after the commissioning of the smelter and were approximately 1.8- and 2.0-fold higher than before smelting periods, respectively. However, air pollution control devices such as Hg reclamation towers and a sulfuric acid plant effectively reduced Hg emissions, as demonstrated by the decrease in THg concentrations despite the increasing production volume after 2000. This work showed the effectiveness of air pollution control measures in reducing Hg emissions into the environment and provided valuable first-hand data to assist with implementing Article 8, Emissions, of the Minamata Convention on Mercury. Based on Hg isotope tracing, this study demonstrates that at the same site, reservoir sediments are more vulnerable to Hg pollution by the Zhuzhou smelter than soil because reservoir sediments receive Hg from the soil with additional Hg input from the Zhuzhou smelter via atmospheric deposition. This highlights the higher risk of Hg pollution in Zhuzhou lakes and reservoirs, given that aquatic systems are hotspots of Hg methylation. Additionally, our results suggest that decades of Pb—Zn smelting have left a substantial amount of legacy Hg in the Zhuzhou area. Therefore, attention must be paid to the risk of legacy Hg, and future efforts must be focused on the remediation of historically polluted soil and sediments.

Declaration of Competing Interest

The authors declare that they have no known competing financial interests or personal relationships that could have appeared to influence the work reported in this paper.

Data availability

Data will be made available on request.

Acknowledgment

This research was supported by the National Natural Science Foundation of China (41931297) and Guizhou Provincial Natural Science Foundation (No. Qian-Ke-He-Ji-Chu-ZK[2021]Zhong-Dian 044). We greatly appreciate Dr. Jiang Liu and Dr. Hongqian Yin for providing assistance in sample collection and determination.

Appendix A. Supplementary data

Supplementary data to this article can be found online at https://doi.org/10.1016/j.chemgeo.2023.121622.

References

An, S., et al., 2022. Understanding heavy metal accumulation in roadside soils along major roads in the Tibet Plateau. Sci. Total Environ. 802, 149865 https://doi.org/10.1016/j.scitotenv.2021.149865.

Appleby, P.G., Oldfield, F., 1978. The calculation of lead-210 dates assuming a constant rate of supply of unsupported ^{210}Pb to the sediment. CATENA 5 (1), 1–8. https://doi.org/10.1016/S0341-8162(78)80002-2.

Bergquist, B.A., Blum, J.D., 2007. Mass-dependent and -independent fractionation of Hg isotopes by photoreduction in aquatic systems. Science 318, 417–420. https://doi.org/10.1126/science.1148050.

Bergquist, B.A., Blum, J.D., 2009. The odds and evens of mercury isotopes: applications of mass-dependent and mass-independent isotope fractionation. Elements 5 (6), 353–357. https://doi.org/10.2113/gselements.5.6.353.

Blum, J.D., et al., 2014. Mercury isotopes in earth and environmental sciences. Annu. Rev. Earth Planet Sci. 42, 249–272. https://doi.org/10.1146/annurev-earth-050212-124107.

Blum, J.D., Bergquist, B.A., 2007. Reporting of variations in the natural isotopic composition of mercury. Anal. Bioanal. Chem. 388 (2), 353–359. https://doi.org/10.1007/s00216-007-1236-9.

Cheng, H., et al., 2014. Geochemical background and baseline value of chemical elements in urban soil in China. Earth Sci. Front. 21 (3), 265–306. https://doi.org/10.13745/j.esf.2014.03.028. (In Chinese).

Demers, J.D., et al., 2013. Mercury isotopes in a forested ecosystem: implications for air-surface exchange dynamics and the global mercury cycle. Glob. Biogeochem. Cycles 27 (1), 222–238. https://doi.org/10.1002/gbc.20021.

Driscoll, C.T., et al., 2013. Mercury as a global pollutant: sources, pathways, and effects. Environ. Sci. Technol. 47 (10), 4967–4983. https://doi.org/10.1021/es305071v.

Estrade, N., et al., 2009. Mercury isotope fractionation during liquid–vapor evaporation experiments. Geochim. Cosmochim. Acta 70 (10), 2693–2711. https://doi.org/10.1016/j.gca.2009.01.024.

Estrade, N., et al., 2011. Tracing and quantifying anthropogenic mercury sources in soils of northern France using isotopic signatures. Environ. Sci. Technol. 45 (4), 1235–1242. https://doi.org/10.1021/es1026823.

Feng, X.B., et al., 2010. Tracing mercury contamination sources in sediments using mercury isotope compositions. Environ. Sci. Technol. 44 (9), 3363–3368. https://doi.org/10.1021/es9039488.

Foucher, D., et al., 2009. Tracing mercury contamination from the Idrija mining region (Slovenia) to the Gulf of Trieste using Hg isotope ratio measurements. Environ. Sci. Technol. 43 (1), 33–39. https://doi.org/10.1021/es801772b.

Janssen, S.E., et al., 2015. Separation of monomethylmercury from estuarine sediments for mercury isotope analysis. Chem. Geol. 411, 19–25. https://doi.org/10.1016/j.chemgeo.2015.06.017.

Jiskra, M., et al., 2012. Solution speciation controls mercury isotope fractionation of Hg (II) sorption to goethite. Environ. Sci. Technol. 46 (12), 6654–6662. https://doi.org/10.1021/es3008112.

Kritee, K., et al., 2013. Microbial stable isotope fractionation of mercury: a synthesis of present understanding and future directions. Chem. Geol. 366, 13–25. https://doi.org/10.1016/j.chemgeo.2012.08.017.

Kurz, A.Y., et al., 2019. Changes in the mercury isotopic composition of sediments from a remote alpine lake in Wyoming, USA. Sci. Total Environ. 669, 973–982. https://doi.org/10.1016/j.scitotenv.2019.03.165.

Kwon, S.Y., et al., 2020. Mercury stable isotopes for monitoring the effectiveness of the Minamata Convention on Mercury. Earth Sci. Rev. 203 https://doi.org/10.1016/j.earscirev.2020.103111.

Lei, M., et al., 2008. Heavy metals pollution and potential ecological risk in paddy soils around mine areas and smelting areas in Hunan Province. Acta Sci. Circumst. 28 (6), 1212–1220. https://doi.org/10.13671/j.hjkxxb.2008.06.028. (In Chinese).

Lepak, R.F., et al., 2020. Resolving atmospheric mercury loading and source trends from isotopic records of remote North American Lake Sediments. Environ. Sci. Technol. 54 (15), 9325–9333. https://doi.org/10.1021/acs.est.0c00579.

Li, Z.G., et al., 2011. Mercury and other metal and metalloid soil contamination near a Pb/Zn smelter in East Hunan province, China. Appl. Geochem. 26 (2), 160–166. https://doi.org/10.1016/j.apgeochem.2010.11.014.

Li, P., et al., 2015. Contamination and health risks of soil heavy metals around a lead/zinc smelter in southwestern China. Ecotoxicol. Environ. Saf. 113, 391–399. https://doi.org/10.1007/s11631-015-0055-5.

Li, X.Y., et al., 2018. Health risks of heavy metal exposure through vegetable consumption near a large-scale Pb/Zn smelter in Central China. Ecotoxicol. Environ. Saf. 161, 99–110. https://doi.org/10.1016/j.ecoenv.2018.05.080.

Liu, J.L., et al., 2011. Mercury distributions and mercury isotope signatures in sediments of Dongjiang, the Pearl River Delta, China. Chem. Geol. 287 (1–2), 81–89. https://doi.org/10.1016/j.chemgeo.2011.06.001.

Liu, F., et al., 2013. Evaluation and source analysis of the mercury pollution in soils and vegetables around a large-scale zinc smelting plant. Environ. Sci. 34 (2), 712–717 (In Chinese).

Ma, J., et al., 2013. Mercury concentrations and mercury isotope composition in lake sediment cores from the vicinity of a metal smelting facility in Flin Flon, Manitoba. Chem. Geol. 336, 96–102. https://doi.org/10.1016/j.chemgeo.2012.10.037.

Perrot, V., et al., 2013. Successive methylation and demethylation of methylated mercury species (MeHg and DMeHg) induce mass dependent fractionation of mercury isotopes. Chem. Geol. 355, 153–162. https://doi.org/10.1016/j.chemgeo.2013.07.011.

Pirrone, N., et al., 2010. Global mercury emissions to the atmosphere from anthropogenic and natural sources. Atmos. Chem. Phys. 10 (13), 5951–5964. https://doi.org/10.5194/acpd-10-4719-2010.

Qin, C.Y., et al., 2020. Isotopic fractionation and source appointment of methylmercury and inorganic mercury in a paddy ecosystem. Environ. Sci. Technol. 54 (22), 14334–14342. https://doi.org/10.1021/acs.est.0c03341.
Sakata, M., Marumoto, K., 2005. Wet and dry deposition fluxes of mercury in Japan. Atmos. Environ. 39 (17), 3139–3146. https://doi.org/10.1016/j.atmosenv.2005.01.049.
Sanchez-Cabeza, J.A., Ruiz-Fernández, A.C., 2012. ^{210}Pb sediment radiochronology: an integrated formulation and classification of dating models. Geochim. Cosmochim. Acta 82, 183–200. https://doi.org/10.1016/j.gca.2010.12.024.
Schneider, L., et al., 2021. Mercury atmospheric emission, deposition and isotopic fingerprinting from major coal-fired power plants in Australia: insights from palaeo-environmental analysis from sediment cores. Environ. Pollut. 287 https://doi.org/10.1016/j.envpol.2021.117596.
Selin, N.E., 2009. Global biogeochemical cycling of mercury: a review. Annu. Rev. Environ. Resour. 34, 43–63. https://doi.org/10.1146/annurev.environ.051308.084314.
Sherman, L., et al., 2010. Mass-independent fractionation of mercury isotopes in Arctic snow driven by sunlight. Nat. Geosci. 3, 173–177. https://doi.org/10.1038/ngeo758.
Sonke, J.E., et al., 2010. Sedimentary mercury stable isotope records of atmospheric and riverine pollution from two major European heavy metal refineries. Chem. Geol. 279 (3–4), 90–100. https://doi.org/10.1016/j.chemgeo.2010.09.017.
Sun, R.Y., et al., 2013. Mercury stable isotope fractionation in six utility boilers of two large coal-fired power plants. Chem. Geol. 336, 103–111. https://doi.org/10.1016/j.chemgeo.2012.10.055.
Sun, G.Y., et al., 2016. Mass-dependent and -independent fractionation of mercury isotope during gas-phase oxidation of elemental mercury vapor by atomic Cl and Br. Environ. Sci. Technol. 50 (17), 9232–9241. https://doi.org/10.1021/acs.est.6b01668.
Sun, R.Y., et al., 2020. Methylmercury produced in upper oceans accumulates in deep Mariana Trench fauna. Nat. Commun. 11, 3389. https://doi.org/10.1038/s41467-020-17045-3.
UNEP, 2019. Global Mercury Assessment 2018. UN Environment Programme, Chemicals and Health Branch Geneva, Switzerland.
Wang, Y.C., et al., 1998. A newly developed sampler for collecting samples near the lacustrine sediment-water interface. Geol. Geochem. 1, 94–96 (In Chinese).
Wang, S.X., et al., 2010. Estimating mercury emissions from a zinc smelter in relation to China's mercury control policies. Environ. Pollut. 158 (10), 3347–3353. https://doi.org/10.1016/j.envpol.2010.07.032.
Wu, Q.R., et al., 2014. Spatial distribution and accumulation of Hg in soil surrounding a Zn/Pb smelter. Sci. Total Environ. 496, 668–677. https://doi.org/10.1016/j.scitotenv.2014.02.067.
Wu, Q.R., et al., 2016. Temporal trend and spatial distribution of speciated atmospheric mercury emissions in China during 1978–2014. Environ. Sci. Technol. 50 (24), 13428–13435. https://doi.org/10.1021/acs.est.6b04308.
Wu, H.C., et al., 2022. Record of heavy metals in Huguangyan Maar Lake sediments: response to anthropogenic atmospheric pollution in Southern China. Sci. Total Environ. 831, 154829 https://doi.org/10.1016/j.scitotenv.2022.154829.
Yin, R.S., et al., 2010a. Application of the stable-isotope system to the study of sources and fate of Hg in the environment: a review. Appl. Geochem. 25 (10), 1467–1477. https://doi.org/10.1016/j.apgeochem.2010.07.007.
Yin, R.S., et al., 2010b. High precision determination of mercury isotope ratios using online mercury vapor generation system coupled with multi-collector inductively coupled plasma-mass spectrometry. Chin. J. Anal. Chem. 38 (7), 929–934. https://doi.org/10.1016/S1872-2040(09)60055-4.
Yin, R.S., et al., 2013a. Mercury speciation and mercury isotope fractionation during ore roasting process and their implication to source identification of downstream sediment in the Wanshan mercury mining area, SW China. Chem. Geol. 336, 72–79. https://doi.org/10.1016/j.chemgeo.2012.04.030.
Yin, R.S., et al., 2013b. Stable mercury isotope variation in rice plants (Oryza sativa L.) from the Wanshan mercury mining district, SW China. Environ. Sci. Technol. 47 (5), 2238–2245. https://doi.org/10.1021/es304302a.
Yin, R.S., et al., 2016. Mercury isotopes as proxies to identify sources and environmental impacts of mercury in sphalerites. Sci. Rep. 6, 18686. https://doi.org/10.1021/acs.est.6b01782.
Yu, B., et al., 2016. Isotopic composition of atmospheric mercury in China: New evidence for sources and transformation processes in air and in vegetation. Environ. Sci. Technol. 50 (17), 9262–9269. https://doi.org/10.1021/acs.est.6b01782.
Zhang, X.W., et al., 2011. Estimation of lead and zinc emissions from mineral exploitation based on characteristics of lead/zinc deposits in China. Trans. Nonferrous Metals Soc. China 21 (11), 2513–2519. https://doi.org/10.1016/S1003-6326(11)61044-3.
Zhang, H., et al., 2013. Atmospheric mercury inputs in montane soils increase with elevation: evidence from mercury isotope signatures. Sci. Rep. 3, 3322. https://doi.org/10.1038/srep03322.
Zheng, W., Hintelmann, H., 2009. Mercury isotope fractionation during photoreduction in natural water is controlled by its Hg/DOC ratio. Geochim. Cosmochim. Acta 73, 6704–6715. https://doi.org/10.1016/j.gca.2009.08.016.
Zheng, W., Hintelmann, H., 2010. Isotope fractionation of mercury during its photochemical reduction by low-molecular-weight organic compounds. J. Phys. Chem. A 114 (12), 4246–4253. https://doi.org/10.1021/jp9111348.
Zheng, W., et al., 2016. Mercury isotope compositions across north American forests. Glob. Biogeochem. Cycles 30 (10), 1475–1492. https://doi.org/10.1002/2015GB005323.
Zheng, W., et al., 2018. Mercury stable isotope fractionation during abiotic dark oxidation in the presence of thiols and natural organic matter. Environ. Sci. Technol. 53 (4), 1853–1862. https://doi.org/10.1021/acs.est.8b05047.